Wave Propagation in Porous Media Saturated with Two Fluids

Is it Feasible to Detect Leakage of a CO_2 Storage Site Using Seismic Waves?

Marc S. Boxberg · Jean H. Prévost · Jeroen Tromp

Abstract When it comes to geological storage of CO_2, monitoring is crucial to detect leakage in the caprock. In our study, we investigated the wave speeds of porous media filled with CO_2 and water in order to determine reservoir changes. We focused on deep storage sites where CO_2 is in a supercritical state. In case of a leak, CO_2 rises and eventually starts to boil as soon as it reaches temperatures or pressures below the critical point. At this point, there are two distinct phases in the pore space. We derived the necessary equations to calculate the wave speeds for unsaturated porous media and tested the equations for a representative storage scenario. We found that there are three modes of pressure waves instead of two for the saturated case. The new mode has a very small wave speed and is highly attenuated. This mode will most likely be very hard to detect in practice and therefore it may be necessary to use time-lapse seismic migration to detect leakage.

1 Introduction

Carbon capture and storage (CCS) or geologic carbon sequestration in general is an attempt to reduce the amount of greenhouse gases emitted to the atmosphere. CO_2 is separated from

M. S. Boxberg (✉) · J. H. Prévost
Department of Civil & Environmental Engineering, Princeton University, Princeton, NJ 08544, USA
e-mail: marc.boxberg@rub.de

M. S. Boxberg
Present address:
Institute of Geology, Mineralogy and Geophysics, Ruhr-University Bochum, 44780 Bochum, Germany

J. Tromp
Department of Geosciences and Program in Applied & Computational Mathematics, Princeton University, Princeton, NJ 08544, USA
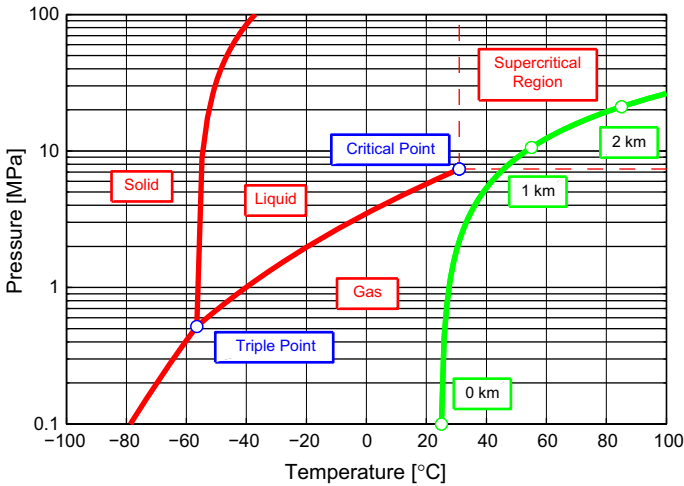
Fig. 1 Phase diagram for pure CO_2 (data from Span and Wagner 1996) including subsurface conditions (*green curve*) assuming a geothermal gradient of $30\,\mathrm{K\,km^{-1}}$, a pressure gradient of $10.5\,\mathrm{MPa\,km^{-1}}$ as well as a surface temperature of $25\,^\circ\mathrm{C}$ and a surface pressure of $0.1\,\mathrm{MPa}$

the flue gas of fossil-fuel power plants or other industries and stored underground. There are three likely underground storage options: injection into depleted oil or gas fields (including enhanced oil recovery), injection into unmineable coal seams, and injection into deep saline aquifers, that is, into highly permeable sandstones that are filled with brine.

Independent of the type of storage, monitoring is crucial. Assuming that after injection of CO_2 into the storage site, suddenly, a leak forms in the caprock (a low permeable seal of the reservoir). How can we detect the leak? In this study, we investigate the wave speeds of porous media filled with CO_2 and water in order to determine changes in the wave speeds and to evaluate whether it is possible to detect a leak with seismic waves.

We focus on deep storage sites where the CO_2 is in a supercritical state, which means that the temperature and pressure have to be above $31.1\,^\circ\mathrm{C}$ and $7.38\,\mathrm{MPa}$. Assuming a geothermal gradient of $30\,\mathrm{K\,km^{-1}}$ and a pressure gradient of $10\,\mathrm{MPa\,km^{-1}}$, the minimum depth for a storage site is $700\,\mathrm{m}$ (see Fig. 1). Statistical investigations by Kopp et al. (2009) show that saline aquifers suitable for CO_2-storage have a median depth of $1524\,\mathrm{m}$, which is the depth we will later use for our calculations.

In case of a leak, CO_2 will rise and start to boil as soon as it reaches temperatures or pressures below the critical point. Therefore, there will be gaseous CO_2 in the pores above this depth. The physical properties of gaseous CO_2 and supercritical CO_2 are very different (especially in terms of density), and thus it is likely that seismic waves propagating through a porous medium filled with gaseous CO_2 and water have different speeds than through media filled with supercritical CO_2 and water or only with water.

Biot (1955, 1956a, b) developed a theory for wave propagation in porous and elastic media, which enables the computation of compressional and shear wave speeds from the physical properties of the fluid that fills the pores and the material that forms the skeleton. Biot's theory is limited to saturated porous media. This work is an extension of Biot's theory to unsaturated porous media. Previously, among others, Albers (2009) and Santos et al. (1990a, b) presented approaches to extend Biot's theory to porous media saturated by two fluids. Albers (2009) used an approach based on a macroscopic linear model, which accommodates both the Biot

model and the Simple Mixture Model of Wilmanski (1998). Santos et al. (1990a) present a Lagrangian derivation using a thermodynamical approach and including the principle of virtual complementary work and energy density functions. The derivation of our equations is loosely based on Coussy (2004).

This paper both presents an approach to extend Biot's theory and intends to answer the question whether it is possible to directly detect leakage of a caprock of a CO_2-storage site by seismic waves. Therefore, we first derive the equations for wave propagation in unsaturated porous media and afterwards use these equations to calculate wave speeds for a leak in the caprock of a storage site at 1524 m depth.

2 Theory

In this section, we derive equations that allow us to calculate wave speeds in unsaturated porous media, i.e., for multiple fluids in the pore space. The procedure is as follows: first, we derive the storage equation for multiple fluids, describing the fluid mass balance; next, we set up the balance of linear momentum and linearize the resulting equations; finally, we determine the wave speeds. For a more detailed introduction into seismic wave propagation and poromechanics, the reader is referred to Aki and Richards (2002) and Coussy (2004), respectively.

2.1 Storage Equation for Multiple Fluids

Consider a porous solid with current pore volume $d\Omega_t^p$ and total volume $d\Omega_t$. The pores are filled with α immiscible fluids f_α whose density is denoted by ρ_{f_α} and whose saturation is denoted by S_{f_α}. The mass balance of the fluids f_α is then given by

$$\frac{d^{f_\alpha}}{dt}\left(\rho_{f_\alpha}\varphi S_{f_\alpha}d\Omega_t\right) = 0, \tag{1}$$

where $\frac{d^{f_\alpha}}{dt}$ is the substantial derivative and φ the Eulerian porosity. For a homogeneous medium, $\nabla S_{f_\alpha} = \nabla\varphi = \nabla\rho_{f_\alpha} = 0$. Therefore, using the product rule and $\frac{d^{f_\alpha}}{dt}d\Omega_t = \nabla \cdot \mathbf{v}^{f_\alpha}d\Omega_t$, where $\mathbf{v}^\beta = \dot{\mathbf{u}}^\beta$ with $\beta = f_\alpha, s$ denotes the velocity of fluid f_α or the solid s, it follows that

$$\rho_{f_\alpha}\frac{\partial}{\partial t}\left(\varphi S_{f_\alpha}\right) + \varphi S_{f_\alpha}\frac{\partial\rho_{f_\alpha}}{\partial t} + \rho_{f_\alpha}\varphi S_{f_\alpha}\nabla \cdot \mathbf{v}^{f_\alpha} = 0. \tag{2}$$

Next, we replace the change in density by the change in pressure using the definition for the bulk modulus K_{f_α} of fluid f_α, namely

$$K_{f_\alpha} = \rho_{f_\alpha}\frac{\partial p_{f_\alpha}}{\partial\rho_{f_\alpha}}, \tag{3}$$

where p_{f_α} is the partial pressure of fluid f_α. Upon insertion of Eq. 3 in Eq. 2, we obtain

$$S_{f_\alpha}\frac{\partial\varphi}{\partial t} + \varphi\frac{\partial S_{f_\alpha}}{\partial t} + \frac{\varphi S_{f_\alpha}}{K_{f_\alpha}}\frac{\partial p_{f_\alpha}}{\partial t} + \varphi S_{f_\alpha}\nabla \cdot \mathbf{v}^{f_\alpha} = 0. \tag{4}$$

In the case of two fluids in a porous medium, a pressure discontinuity, caused by interfacial interactions, occurs. Neglecting hysteresis effects, this capillary pressure $p_c = p_{f_1} - p_{f_2}$ can be described as a unique function under isothermal conditions (Lo et al. 2005). The change in capillary pressure with time can be expressed as

$$\frac{\partial p_c}{\partial t} = \frac{\mathrm{d} p_c}{\mathrm{d} S_{f_\alpha}} \frac{\partial S_{f_\alpha}}{\partial t} = \frac{\partial p_1}{\partial t} - \frac{\partial p_2}{\partial t}. \tag{5}$$

Therefore, the change in saturation of one fluid phase can be expressed as

$$\frac{\partial S_{f_\alpha}}{\partial t} = \frac{\mathrm{d} S_{f_\alpha}}{\mathrm{d} p_c} \left(\frac{\partial p_1}{\partial t} - \frac{\partial p_2}{\partial t} \right). \tag{6}$$

The capillary pressure curve $\left(\text{i.e.,} \ \frac{\mathrm{d} p_c}{\mathrm{d} S_{f_1}} \left(S_{f_1} \right) \right)$ can be described using the model of van Genuchten (1980):

$$\frac{\mathrm{d} S_{f_1}}{\mathrm{d} p_c} = \frac{\rho_2 g}{mn\chi} \left[\left(1 - S_{f_1} \right)^{-\frac{1}{m}} - 1 \right]^{\frac{1}{n}-1} \left(1 - S_{f_1} \right)^{-\left(\frac{1}{m} + 1 \right)}, \tag{7}$$

where n and χ are fitting parameters and $m = 1 - \frac{1}{n}$.

The incremental state equation (Coussy 2004) is given by

$$\frac{\mathrm{d}\varphi}{\mathrm{d} t} = (b - \varphi) \, \mathbf{\nabla} \cdot \mathbf{v}^s + \frac{1}{N} \frac{\mathrm{d} p_f}{\mathrm{d} t} - 3\alpha_s (b - \phi_0) \frac{\mathrm{d} T}{\mathrm{d} t}, \tag{8}$$

where $N = \frac{K_s}{b-\varphi}$, with the bulk modulus of the rock denoted by K_s. This equation relates the change in porosity to the strain variation, the change in pressure, and the change in temperature. We neglect the term for the volumetric thermal dilation $\left(-3\alpha_s (b - \phi_0) \frac{\mathrm{d} T}{\mathrm{d} t} \right)$ because we assume the temperature to be constant and insert this equation, as well as Eq. 6 into Eq. 4. Writing this equation explicitly for two fluids $\alpha = 1, 2$ using $\frac{\partial S_2}{\partial t} = -\frac{\partial S_1}{\partial t}$ and solving for $\frac{\partial p_{f_1}}{\partial t}$ and $\frac{\partial p_{f_2}}{\partial t}$ yields

$$\begin{aligned}
\frac{\partial p_{f_1}}{\partial t} = -M \Bigg\{ & K_{f_1} N \left(K_{f_2} \frac{\mathrm{d} S_{f_1}}{\mathrm{d} p_c} + S_{f_1} S_{f_2} \right) (b - \varphi) \, \mathbf{\nabla} \cdot \mathbf{v}_s \\
& + K_{f_1} S_{f_1} \left[S_{f_2} N\varphi + K_{f_2} \left(S_{f_2}^2 + N\varphi \frac{\mathrm{d} S_{f_1}}{\mathrm{d} p_c} \right) \right] \mathbf{\nabla} \cdot \mathbf{v}_{f_1} \\
& + K_{f_1} K_{f_2} S_{f_2} \left(N\varphi \frac{\mathrm{d} S_{f_1}}{\mathrm{d} p_c} - S_{f_1} S_{f_2} \right) \mathbf{\nabla} \cdot \mathbf{v}_{f_2} \Bigg\}
\end{aligned} \tag{9}$$

$$\begin{aligned}
\frac{\partial p_{f_2}}{\partial t} = -M \Bigg\{ & K_{f_2} N \left(K_{f_1} \frac{\mathrm{d} S_{f_1}}{\mathrm{d} p_c} + S_{f_1} S_{f_2} \right) (b - \varphi) \, \mathbf{\nabla} \cdot \mathbf{v}_s \\
& + K_{f_1} K_{f_2} S_{f_1} \left(N\varphi \frac{\mathrm{d} S_{f_1}}{\mathrm{d} p_c} - S_{f_1} S_{f_2} \right) \mathbf{\nabla} \cdot \mathbf{v}_{f_1} \\
& + K_{f_2} S_{f_2} \left[S_{f_1} N\varphi + K_{f_1} \left(S_{f_1}^2 + N\varphi \frac{\mathrm{d} S_{f_1}}{\mathrm{d} p_c} \right) \right] \mathbf{\nabla} \cdot \mathbf{v}_{f_2} \Bigg\},
\end{aligned} \tag{10}$$

with

$$\begin{aligned}
\frac{1}{M} = & \ S_{f_1} S_{f_2} \left(S_{f_1} K_{f_1} + S_{f_2} K_{f_2} + N\varphi \right) \\
& + \left(K_{f_2} S_{f_1} N\varphi + K_{f_1} K_{f_2} + K_{f_1} S_{f_2} N\varphi \right) \frac{\mathrm{d} S_{f_1}}{\mathrm{d} p_c}.
\end{aligned} \tag{11}$$

This equation can be reduced to the equation for the saturated case by setting $S_{f_1} = 1$ and $S_{f_1} = 0$:

$$\frac{\mathrm{d} p_f}{\mathrm{d} t} = -M \left\{ \mathbf{\nabla} \cdot \left[(b - \varphi) \, \mathbf{v}^s \right] + \mathbf{\nabla} \left(\varphi \mathbf{v}^f \right) \right\}, \tag{12}$$

with

$$\frac{1}{M} = \frac{1}{N} + \frac{\varphi}{K_f}. \tag{13}$$

2.2 Balance of Momentum

The balance of linear momentum may be written as

$$\boldsymbol{\nabla} \cdot \left[(1 - \varphi)\, \boldsymbol{\sigma}^{\mathrm{s}}\right] + (1 - \varphi)\, \rho_{\mathrm{s}} \left(\mathbf{b} - \mathbf{a}^{\mathrm{s}}\right) + \mathbf{f}^{\rightarrow \mathrm{s}} = \mathbf{0}, \tag{14}$$

$$\boldsymbol{\nabla} \cdot \left(\varphi S_{f_\alpha} \boldsymbol{\sigma}^{f_\alpha}\right) + \varphi S_{f_\alpha} \rho_{f_\alpha} \left(\mathbf{b} - \mathbf{a}^{f_\alpha}\right) + \mathbf{f}^{\rightarrow f_\alpha} = \mathbf{0}, \tag{15}$$

for the solid part, s, and the fluids, f_α, respectively, where $\boldsymbol{\sigma}^{\mathrm{s}}$ denotes the partial stress tensor of the solid, $\boldsymbol{\sigma}^{f_\alpha}$ the partial stress tensor of fluid f_α, $\mathbf{b}$ the body force per unit mass, $\mathbf{a}^{s}$ and $\mathbf{a}^{f_\alpha}$ the solid and fluid acceleration, respectively, and $\mathbf{f}^{\rightarrow \mathrm{s}}$ and $\mathbf{f}^{\rightarrow f_\alpha}$ capture the interaction with the solid and the fluids, respectively. These interactions have to be balanced, so the momentum transfer is given by

$$\mathbf{f}^{\rightarrow \mathrm{s}} + \sum_\alpha \mathbf{f}^{\rightarrow f_\alpha} = \mathbf{0}. \tag{16}$$

2.2.1 Fluids

The extended Darcy's law is given by

$$\varphi S_{f_\alpha} \left(\mathbf{v}^{f_\alpha} - \mathbf{v}^{\mathrm{s}}\right) = -\boldsymbol{\lambda}_{f_\alpha} \cdot \left[\boldsymbol{\nabla} p_{f_\alpha} - \rho_{f_\alpha} \left(\mathbf{b} - \mathbf{a}^{f_\alpha}\right)\right], \tag{17}$$

with

$$\boldsymbol{\lambda}_{f_\alpha} = \frac{k_{\mathrm{r}, f_\alpha} \mathbf{k}}{\mu_{f_\alpha}}, \tag{18}$$

where $\boldsymbol{\lambda}_{f_\alpha}$ and μ_{f_α} are the mobility tensor and the viscosity of the fluid f_α, respectively, and $\mathbf{k}$ is the permeability tensor of the skeleton (compare to Neumann 1977). $k_{\mathrm{r}, f_\alpha} = k_{\mathrm{r}, f_\alpha}\left(S_{f_\alpha}\right)$ is the saturation-dependent relative permeability. The most commonly used hydraulic conductivity models are those by Brooks and Corey (1964) and van Genuchten (1980). In this work, the model by van Genuchten (1980) is used, where the relative permeability is given by

$$k_{\mathrm{r}, f_\alpha} \left(S_{f_\alpha}\right) = \sqrt{S_{f_\alpha}} \left[1 - \left(1 - S_{f_\alpha}^{\frac{1}{m}}\right)^m\right]^2, \tag{19}$$

with the fitting parameters m and n, related by $m = 1 - \frac{1}{n}$.

We insert Darcy's law into the balance of linear momentum for the fluids (Eq. 15) to obtain

$$\mathbf{f}^{\rightarrow f_\alpha} = S_{f_\alpha} \left[-\varphi^2 S_{f_\alpha} \boldsymbol{\lambda}_{f_\alpha}^{-1} \cdot \left(\mathbf{v}^{f_\alpha} - \mathbf{v}^{\mathrm{s}}\right) + p_{f_\alpha} \boldsymbol{\nabla}\varphi\right] + \varphi p_{f_\alpha} \boldsymbol{\nabla} S_{f_\alpha}. \tag{20}$$

Upon insertion of the last equation into Eq. 15, we obtain the balance of linear momentum for the fluids f_α:

$$-\varphi S_{f_\alpha} \boldsymbol{\nabla} p_{f_\alpha} + \varphi^2 S_{f_\alpha}^2 \boldsymbol{\lambda}_{f_\alpha}^{-1} \left(\mathbf{v}^{\mathrm{s}} - \mathbf{v}^{f_\alpha}\right) + \varphi S_{f_\alpha} \rho_{f_\alpha} \mathbf{b} = \varphi S_{f_\alpha} \rho_{f_\alpha} \mathbf{a}^{f_\alpha}. \tag{21}$$

2.2.2 Solid

Writing out the momentum transfer (Eq. 16) and inserting Eqs. 14 and 20 yields

$$(1 - \varphi)\,\rho_s \mathbf{a}^s = \nabla \cdot \left[(1 - \varphi)\,\boldsymbol{\sigma}^s\right] - p_f \nabla \varphi + \varphi^2 \sum_\alpha S_{f_\alpha}^2 \boldsymbol{\lambda}_{f_\alpha}^{-1} \cdot \left(\mathbf{v}^{f\alpha} - \mathbf{v}^s\right)$$
$$- \varphi \sum_\alpha p_{f_\alpha} \nabla S_{f_\alpha} + (1 - \varphi)\,\rho_s \mathbf{b}. \tag{22}$$

According to Biot (1955), the total stress is given by

$$\boldsymbol{\sigma} = \boldsymbol{\sigma}^{\prime s} - b p_f \mathbf{I}, \tag{23}$$

where $\boldsymbol{\sigma}$ denotes the total stress, $\boldsymbol{\sigma}^{\prime s}$ the effective stress, $\mathbf{I}$ the identity tensor, and b is Biot's coefficient, which depends on the compressibility of the solid matrix and is defined by

$$b = 1 - \frac{K^s}{K_s}. \tag{24}$$

Here, K^s denotes the bulk modulus of the matrix and K_s denotes the bulk modulus of the grains. By using this expression and the definition of the partial stress

$$\boldsymbol{\sigma} = (1 - \varphi)\,\boldsymbol{\sigma}^s + \varphi \boldsymbol{\sigma}^f = (1 - \varphi)\,\boldsymbol{\sigma}^s - \varphi p_f \mathbf{I}, \tag{25}$$

we finally obtain the balance of linear momentum for the solid:

$$(1 - \varphi)\,\rho_s \mathbf{a}^s = \nabla \boldsymbol{\sigma}^{\prime s} - \psi \nabla p_f - \varphi^2 \sum_\alpha S_{f_\alpha}^2 \boldsymbol{\lambda}_{f_\alpha}^{-1} \cdot \left(\mathbf{v}^s - \mathbf{v}^{f\alpha}\right)$$
$$- \varphi \sum_\alpha p_{f_\alpha} \nabla S_{f_\alpha} + (1 - \varphi)\,\rho_s \mathbf{b}. \tag{26}$$

For convenience, we have defined

$$\psi = \psi(\varphi) \equiv b - \varphi. \tag{27}$$

2.3 Linearization of the Balance of Linear Momentum

To linearize the balance of momentum, we need to integrate the storage equation (Eqs. 9 and 10) to obtain an expression for the partial pressure $p_{f_\alpha}, \alpha = 1, 2$. We neglect the body forces $\mathbf{b}$ and assume small fluid and solid motions. Thus, we obtain

$$p_{f_1} = p_{f_1,0} + M \left\{ -K_{f_1} N \left(K_{f_2} \frac{\mathrm{d}S_{f_1}}{\mathrm{d}p_c} + S_{f_1} S_{f_2} \right) \psi \nabla \cdot \mathbf{u}_s \right.$$
$$+ K_{f_1} S_{f_1} \left[S_{f_2} N \varphi + K_{f_2} \left(S_{f_2}^2 + N \varphi \frac{\mathrm{d}S_{f_1}}{\mathrm{d}p_c} \right) \right] \nabla \cdot \mathbf{u}_{f_1}$$
$$\left. + K_{f_1} K_{f_2} S_{f_2} \left(N \varphi \frac{\mathrm{d}S_{f_1}}{\mathrm{d}p_c} - S_{f_1} S_{f_2} \right) \nabla \cdot \mathbf{u}_{f_2} \right\} \tag{28}$$

$$p_{f_2} = p_{f_2,0} + M \left\{ -K_{f_1} N \left(K_{f_1} \frac{\mathrm{d}S_{f_1}}{\mathrm{d}p_c} + S_{f_1} S_{f_2} \right) \psi \nabla \cdot \mathbf{u}_s \right.$$
$$+ K_{f_1} K_{f_2} S_{f_1} \left(N \varphi \frac{\mathrm{d}S_{f_1}}{\mathrm{d}p_c} - S_{f_1} S_{f_2} \right) \nabla \cdot \mathbf{u}_{f_1}$$
$$\left. + K_{f_2} S_{f_2} \left[S_{f_1} N \varphi + K_{f_1} \left(S_{f_1}^2 + N \varphi \frac{\mathrm{d}S_{f_1}}{\mathrm{d}p_c} \right) \right] \nabla \cdot \mathbf{u}_{f_2} \right\}. \tag{29}$$

We substitute these equations into Eq. 21 to obtain the linearized balance of linear momentum of the fluids

$$
\begin{aligned}
& MNK_{f_1}S_{f_1}\left(K_{f_2}\frac{\mathrm{d}S_{f_1}}{\mathrm{d}p_c}+S_{f_1}S_{f_2}\right)\varphi\psi\nabla\left(\nabla\cdot\mathbf{u}_s\right) \\
& +MK_{f_1}S_{f_1}^2\left[K_{f_2}S_{f_2}^2+N\varphi\left(K_{f_2}\frac{\mathrm{d}S_{f_1}}{\mathrm{d}p_c}+S_{f_2}\right)\right]\varphi\nabla\left(\nabla\cdot\mathbf{u}_{f_1}\right) \\
& +MK_{f_1}K_{f_2}S_{f_1}S_{f_2}\left(N\varphi\frac{\mathrm{d}S_{f_1}}{\mathrm{d}p_c}-S_{f_1}S_{f_2}\right)\varphi\nabla\left(\nabla\cdot\mathbf{u}_{f_2}\right) \\
& +\varphi^2 S_{f_1}^2\boldsymbol{\lambda}_{f_1}^{-1}\frac{\partial\mathbf{u}_s}{\partial t}-\varphi^2 S_{f_1}^2\boldsymbol{\lambda}_{f_1}^{-1}\frac{\partial\mathbf{u}_{f_1}}{\partial t}-\varphi S_{f_1}\rho_{f_1}\frac{\partial^2\mathbf{u}_{f_1}}{\partial t^2}=0
\end{aligned}
\tag{30}
$$

$$
\begin{aligned}
& MNK_{f_2}S_{f_2}\left(K_{f_1}\frac{\mathrm{d}S_{f_1}}{\mathrm{d}p_c}+S_{f_1}S_{f_2}\right)\varphi\psi\nabla\left(\nabla\cdot\mathbf{u}_s\right) \\
& +MK_{f_1}K_{f_2}S_{f_1}S_{f_2}\left(N\varphi\frac{\mathrm{d}S_{f_1}}{\mathrm{d}p_c}-S_{f_1}S_{f_2}\right)\varphi\nabla\left(\nabla\cdot\mathbf{u}_{f_1}\right) \\
& +MK_{f_2}S_{f_2}^2\left[K_{f_1}S_{f_1}^2+N\varphi\left(K_{f_1}\frac{\mathrm{d}S_{f_1}}{\mathrm{d}p_c}+S_{f_1}\right)\right]\varphi\nabla\left(\nabla\cdot\mathbf{u}_{f_2}\right) \\
& +\varphi^2 S_{f_2}^2\boldsymbol{\lambda}_{f_2}^{-1}\frac{\partial\mathbf{u}_s}{\partial t}-\varphi^2 S_{f_2}^2\boldsymbol{\lambda}_{f_2}^{-1}\frac{\partial\mathbf{u}_{f_2}}{\partial t}-\varphi S_{f_2}\rho_{f_2}\frac{\partial^2\mathbf{u}_{f_2}}{\partial t^2}=0.
\end{aligned}
\tag{31}
$$

We also substitute the linearized storage equation (Eqs. 28 and 29) into the equation that describes the balance of linear momentum of the solid (Eq. 26). In addition, we use Hooke's law and the Lamé moduli λ^s and μ^s for isotropic media to replace the stress tensor $\boldsymbol{\sigma}'^s$ by the displacement gradients $\nabla\mathbf{u}^s$ according to

$$
\boldsymbol{\sigma}'^s=\mathbf{E}^s:\boldsymbol{\varepsilon}^s=2\mu^s\boldsymbol{\varepsilon}^s+\lambda^s\mathrm{tr}\left(\boldsymbol{\varepsilon}^s\right)\mathbf{I}
\tag{32}
$$
$$
\nabla\boldsymbol{\sigma}'^s=\left(\lambda^s+2\mu^s\right)\nabla\left(\nabla\cdot\mathbf{u}^s\right)-\mu^s\nabla\times\left(\nabla\times\mathbf{u}^s\right),
\tag{33}
$$

where $\mathbf{E}^s$ denotes the elastic tensor and $\boldsymbol{\varepsilon}^s$ the linear strain tensor (compare to Jeffreys and Jeffreys 1950). Thus, we finally obtain the linearized balance of linear momentum equation for the solid:

$$
\begin{aligned}
& \left\{\lambda^s+2\mu^s+MN\left[K_{f_1}K_{f_2}\frac{\mathrm{d}S_{f_1}}{\mathrm{d}p_c}+S_{f_1}S_{f_2}\left(K_{f_1}S_{f_1}+K_{f_2}S_{f_2}\right)\right]\psi^2\right\}\nabla\left(\nabla\cdot\mathbf{u}_s\right) \\
& +MNK_{f_1}S_{f_1}\left(S_{f_1}S_{f_2}+K_{f_2}\frac{\mathrm{d}S_{f_1}}{\mathrm{d}p_c}\right)\varphi\psi\nabla\left(\nabla\cdot\mathbf{u}_{f_1}\right) \\
& +MNK_{f_2}S_{f_2}\left(S_{f_1}S_{f_2}+K_{f_1}\frac{\mathrm{d}S_{f_1}}{\mathrm{d}p_c}\right)\varphi\psi\nabla\left(\nabla\cdot\mathbf{u}_{f_2}\right) \\
& -\varphi^2\left(S_{f_1}\boldsymbol{\lambda}_{f_1}^{-1}+S_{f_2}\boldsymbol{\lambda}_{f_2}^{-1}\right)\cdot\frac{\partial\mathbf{u}_s}{\partial t}+\varphi^2 S_{f_1}\boldsymbol{\lambda}_{f_1}^{-1}\cdot\frac{\partial\mathbf{u}_{f_1}}{\partial t}+\varphi^2 S_{f_2}\boldsymbol{\lambda}_{f_2}^{-1}\cdot\frac{\partial\mathbf{u}_{f_2}}{\partial t} \\
& -(1-\varphi)\rho_s\frac{\partial^2\mathbf{u}_s}{\partial t^2}-\mu^s\nabla\times\left(\nabla\times\mathbf{u}_s\right)=0.
\end{aligned}
\tag{34}
$$

2.4 Propagation of Harmonic Waves

2.4.1 Longitudinal Waves

Let us consider the propagation of harmonic longitudinal waves in the $\mathbf{e}_x$ direction:

$$\mathbf{u}^s = u_0^s \text{Re}\left\{\exp\left[i\left(sx + \omega t\right)\right]\right\} \mathbf{e}_x, \tag{35}$$

$$\mathbf{u}^{f_\alpha} = u_0^{f_\alpha} \text{Re}\left\{\exp\left[i\left(sx + \omega t\right)\right]\right\} \mathbf{e}_x, \tag{36}$$

where s denotes the wave number and ω denotes the angular frequency.

2.4.1.1 Two Fluids Substituting this into Eqs. 30, 31, and 34 yields

$$\left(-s^2 \mathsf{S} + i\omega \mathsf{K} + \omega^2 \mathsf{M}\right) \cdot \begin{pmatrix} u_0^s \\ u_0^{f_1} \\ u_0^{f_2} \end{pmatrix} = 0, \tag{37}$$

with the stiffness matrix S, the damping matrix K, and the mass matrix M defined as

$$\mathsf{S} = \begin{pmatrix} \mathsf{s}_{11} & \mathsf{s}_{12} & \mathsf{s}_{13} \\ \mathsf{s}_{21} & \mathsf{s}_{22} & \mathsf{s}_{23} \\ \mathsf{s}_{31} & \mathsf{s}_{32} & \mathsf{s}_{33} \end{pmatrix}, \tag{38}$$

$$\mathsf{K} = \varphi^2 \begin{pmatrix} -\left(\dfrac{S_{f_1}^2}{\lambda_{f_1}} + \dfrac{S_{f_2}^2}{\lambda_{f_2}}\right) & \dfrac{S_{f_1}^2}{\lambda_{f_1}} & \dfrac{S_{f_2}^2}{\lambda_{f_2}} \\[2mm] \dfrac{S_{f_1}^2}{\lambda_{f_1}} & -\dfrac{S_{f_1}^2}{\lambda_{f_1}} & 0 \\[2mm] \dfrac{S_{f_2}^2}{\lambda_{f_2}} & 0 & -\dfrac{S_{f_2}^2}{\lambda_{f_2}} \end{pmatrix}, \tag{39}$$

$$\mathsf{M} = \begin{pmatrix} (1-\varphi)\,\rho_s & 0 & 0 \\ 0 & \varphi S_{f_1}\rho_{f_1} & 0 \\ 0 & 0 & \varphi S_{f_2}\rho_{f_2} \end{pmatrix}. \tag{40}$$

$$\mathsf{s}_{11} = \lambda^s + 2\mu^s + MN\left[K_{f_1}K_{f_2}\frac{\mathrm{d}S_{f_1}}{\mathrm{d}p_c} + S_{f_1}S_{f_2}\left(K_{f_1}S_{f_1} + K_{f_2}S_{f_2}\right)\right]\psi^2 \tag{41}$$

$$\mathsf{s}_{22} = MK_{f_1}S_{f_1}^2\left[K_{f_2}S_{f_2}^2 + N\varphi\left(K_{f_2}\frac{\mathrm{d}S_{f_1}}{\mathrm{d}p_c} + S_{f_2}\right)\right]\varphi \tag{42}$$

$$\mathsf{s}_{33} = MK_{f_2}S_{f_2}^2\left[K_{f_1}S_{f_1}^2 + N\varphi\left(K_{f_1}\frac{\mathrm{d}S_{f_1}}{\mathrm{d}p_c} + S_{f_1}\right)\right]\varphi \tag{43}$$

$$\mathsf{s}_{12} = \mathsf{s}_{21} = MNK_{f_1}S_{f_1}\left(K_{f_2}\frac{\mathrm{d}S_{f_1}}{\mathrm{d}p_c} + S_{f_1}S_{f_2}\right)\varphi\psi \tag{44}$$

$$\mathsf{s}_{13} = \mathsf{s}_{31} = MNK_{f_2}S_{f_2}\left(K_{f_1}\frac{\mathrm{d}S_{f_1}}{\mathrm{d}p_c} + S_{f_1}S_{f_2}\right)\varphi\psi \tag{45}$$

$$\mathsf{s}_{23} = \mathsf{s}_{32} = MK_{f_1}K_{f_2}S_{f_1}S_{f_2}\left(N\varphi\frac{\mathrm{d}S_{f_1}}{\mathrm{d}p_c} - S_{f_1}S_{f_2}\right)\varphi \tag{46}$$

To obtain the dispersion relation for the harmonic longitudinal waves, we have to solve the following equation for wave number s as a function of frequency ω:

$$\det\left(-s^2\mathsf{S} + i\omega\mathsf{K} + \omega^2\mathsf{M}\right) = 0. \tag{47}$$

The resulting s reveals both the speed for the longitudinal waves $c = \frac{\omega}{\text{Re}(s)}$ and the corresponding attenuation coefficient $\alpha = \text{Im}(s)$.

4.2.1.2 One Fluid We can also obtain the well-known equation for fluid-saturated porous media (e.g., Coussy 2004). For the saturated case, we only consider one fluid and the corresponding saturation is $S_f = 1$. Therefore, we find

$$\left(-s^2 \mathsf{S} + i\omega \mathsf{K} + \omega^2 \mathsf{M}\right) \cdot \begin{pmatrix} u_0^s \\ u_0^f \end{pmatrix} = 0. \tag{48}$$

In this case, the stiffness matrix S, damping matrix K, and mass matrix M are defined by

$$\mathsf{S} = \begin{pmatrix} \lambda^s + 2\mu^s + \psi^2 M & \varphi\psi M \\ \varphi\psi M & \varphi^2 M \end{pmatrix}, \tag{49}$$

$$\mathsf{K} = \frac{\varphi^2}{\lambda_f} \begin{pmatrix} -1 & 1 \\ 1 & -1 \end{pmatrix}, \tag{50}$$

$$\mathsf{M} = \begin{pmatrix} (1-\varphi)\rho_s & 0 \\ 0 & \varphi\rho_f \end{pmatrix}. \tag{51}$$

2.4.2 Transverse Waves

Let us now consider the propagation of harmonic transverse waves traveling in the $\mathbf{e}_y$ direction and polarized in the $\mathbf{e}_x$ direction:

$$\mathbf{u}^s = u_0^s \text{Re}\{\exp[i(sy + \omega t)]\}\mathbf{e}_x \tag{52}$$

$$\mathbf{u}^{f_\alpha} = u_0^{f_\alpha} \text{Re}\{\exp[i(sy + \omega t)]\}\mathbf{e}_x. \tag{53}$$

4.2.2.1 Two Fluids Substituting this into Eqs. 30, 31, and 34 yields

$$\left(-s^2 \mathsf{T} + i\omega \mathsf{K} + \omega^2 \mathsf{M}\right) \cdot \begin{pmatrix} u_0^s \\ u_0^{f_1} \\ u_0^{f_2} \end{pmatrix} = 0 \tag{54}$$

with the damping and mass matrices defined according to Eqs. 39 and 40 and the matrix T defined by

$$\mathsf{T} = \begin{pmatrix} \mu^s & 0 & 0 \\ 0 & 0 & 0 \\ 0 & 0 & 0 \end{pmatrix}. \tag{55}$$

To obtain the dispersion relation for the harmonic transverse waves, we have to solve the following equation for the wave number s as a function of the frequency ω:

$$\det\left(-s^2 \mathsf{T} + i\omega \mathsf{K} + \omega^2 \mathsf{M}\right) = 0. \tag{56}$$

The resulting s reveals both the speed for the transverse wave $c = \frac{\omega}{\text{Re}(s)}$ and the corresponding attenuation coefficient $\alpha = \text{Im}(s)$.

2.4.2.2 One Fluid For the case of one fluid we have

$$\left(-s^2 \mathsf{T} + i\omega \mathsf{K} + \omega^2 \mathsf{M}\right) \cdot \begin{pmatrix} u_0^s \\ u_0^f \end{pmatrix} = 0 \tag{57}$$

Table 1 Depth-independent physical properties used for the calculation of wave speeds

Parameter	Symbol	Value
General		
Biot's coefficient	b	1
Porosity	φ	0.2
Lamé's first parameter	λ^s	6.67 GPa
Shear modulus	μ^s	6.67 GPa
Permeability	k	1 D
Acceleration of gravity	g	9.81 m s^{-2}
Fitting parameter	n	2.28
Fitting parameter	χ	0.69 m^{-1}
Rock		
Bulk modulus	K_s	1,000 MPa
Density	ρ_s	2,600 kg m^{-3}
Water		
Bulk modulus	K_{H_2O}	2170 MPa
Viscosity	μ_{H_2O}	1×10^{-3} Pa s
Density	ρ_{H_2O}	1025.5 kg m^{-3}
CO$_2$		
Bulk modulus	K_{CO_2}	0.4 MPa
Viscosity	μ_{CO_2}	2×10^{-5} Pa s

with the damping and mass matrices defined according to Eqs. 50 and 51 and with the matrix T defined by

$$\mathsf{T} = \begin{pmatrix} \mu^s & 0 \\ 0 & 0 \end{pmatrix}. \tag{58}$$

3 Application

Having obtained the necessary equations for calculating wave speeds in unsaturated porous media, we apply our theory for a representative storage site. Kopp et al. (2009) determined characteristic parameters for typical reservoirs using statistical calculations based on a database of more than 1,200 reservoirs. They found that an average reservoir has a depth of 1,524 m with a reservoir pressure of 15.47 MPa at a temperature of 55.13 °C. The density of the water therein is 1025.5 kg m^{-3}. With these values, we calculated the density and saturation of CO$_2$ as well as the saturation of water for various depths, starting at 1,524 m, using a flash calculation (Gor and Prévost 2014; Prévost 1981). The capillary pressure curve of a CO$_2$/water system was measured by e.g., Plug and Bruining (2007) and Pini et al. (2012). We calibrated the capillary pressure curve model by van Genuchten (1980), which was given in Eq. 7, with the data presented by Pini et al. (2012) and obtained $n = 2.28$ and $\chi = 0.69$ m^{-1}. These and all other values used are listed in Tables 1 and 2. We used our equations for wave speeds and attenuation of longitudinal (Eq. 47) and transverse waves (Eq. 56) to determine profiles as a function of depth h and frequency ω.

**Table 2** Depth-dependent properties used in the calculation

h (m)	p (MPa)	T (°C)	S_{CO_2} (–)	S_{H_2O} (–)	ρ_{CO_2} (kg m^{-3})
1,524	15.47	55.13	0.75000	0.25000	653.99
1,500	15.24	54.42	0.75021	0.24979	653.43
1,400	14.23	51.45	0.75156	0.24844	649.31
1,300	13.22	48.49	0.75313	0.24687	644.49
1,200	12.21	45.53	0.75495	0.24505	638.83
1,100	11.20	42.57	0.75714	0.24286	631.94
1,000	10.19	39.61	0.75988	0.24012	623.18
900	9.18	36.65	0.76360	0.23640	611.13
800	8.17	33.69	0.76945	0.23055	591.98
722	7.38	31.38	0.77912	0.22088	560.27
708	7.24	30.96	0.78244	0.21756	549.47
700	7.16	30.73	0.78552	0.21448	539.48
696	7.12	30.61	0.78751	0.21249	533.07
695	7.11	30.58	0.86984	0.13016	294.33
650	6.66	29.25	0.89304	0.10696	235.70
600	6.15	27.77	0.90962	0.09038	195.70
500	5.15	24.81	0.93277	0.06723	142.29
400	4.14	21.84	0.95054	0.04946	103.00
300	3.13	18.88	0.96523	0.03477	71.51
200	2.12	15.92	0.97789	0.02211	45.04
100	1.11	12.96	0.98906	0.01094	22.12

Depth is denoted by h. Pressure p and temperature T are calculated using a pressure gradient of 10.09 MPa km^{-1} and a geothermal gradient of 29.61 °C km^{-1}, as well as a surface temperature T_0 of 10 °C. Saturation of CO_2 S_{CO_2} and water S_{H_2O} and the density of CO_2 ρ_{CO_2} are calculated based on the approach of Gor and Prévost (2014)

4 Results

We found that there is a third mode pressure wave in porous media saturated by two immiscible, whereas there are only two modes of pressure waves in porous media saturated by only one fluid. This was also observed in previous studies (e.g., Santos et al. 1990a, b; Lo et al. 2005; Albers 2009). We have a first mode pressure wave (P_1), where the solid and fluids are in phase; a second mode pressure wave (P_2), where the solid and the fluids move out of phase; and a third mode pressure wave (P_3), where the fluids move in phase but not in phase with the solid. The additional wave, compared to the case of one fluid is P_2. For every additional fluid there would be an additional pressure wave phase, because the dimension of the matrices is $(\alpha + 1) \times (\alpha + 1)$ (see Eqs. 47 and 56) and the number of solutions is $(\alpha + 1)$.

To compare the differences between the saturated case, where all pores are filled with water, and the unsaturated case, where there is CO_2 and water in the pore space, we compared these two cases at 600 m depth (see Fig. 2). This leads us to several interesting observations: P_1 is about 15% slower in the case where CO_2 is present compared to the case where there is only water in the pores, whereas P_2 is about 95% slower in the case where CO_2 is present. The additional P_3 wave is extraordinary slow and highly attenuated. The transverse S wave is not
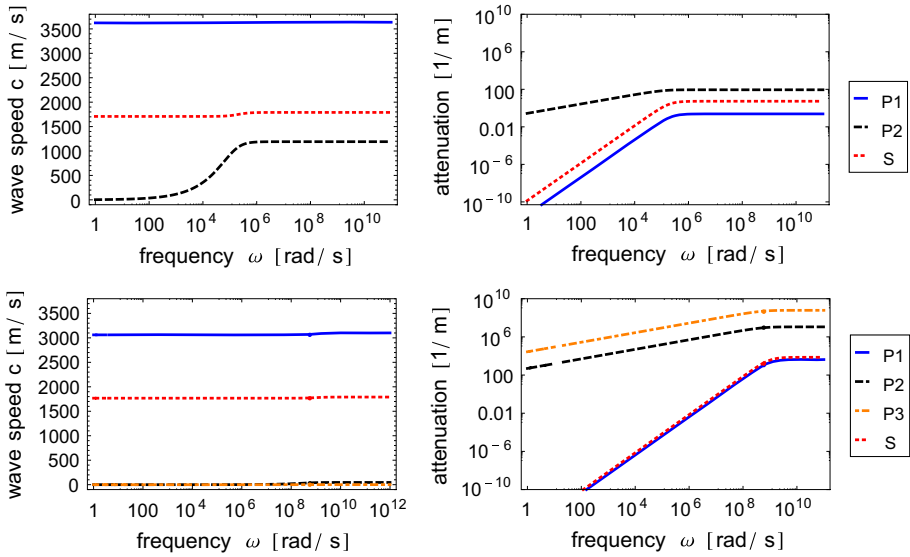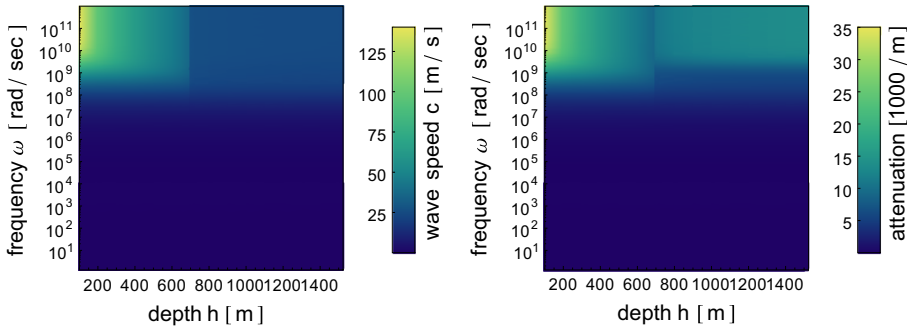
Fig. 2 Wave speeds (*left*) and attenuation (*right*) of the seismic waves at a depth of 600 m. The *upper plots* are calculated using the equations for the saturated case and the *lower plots* are calculated using the equations for the unsaturated case
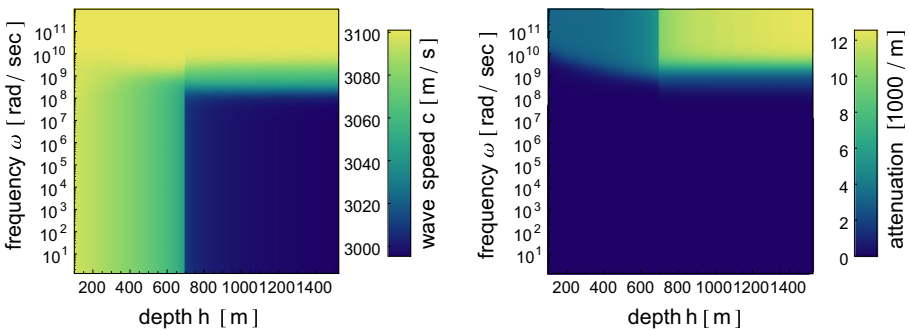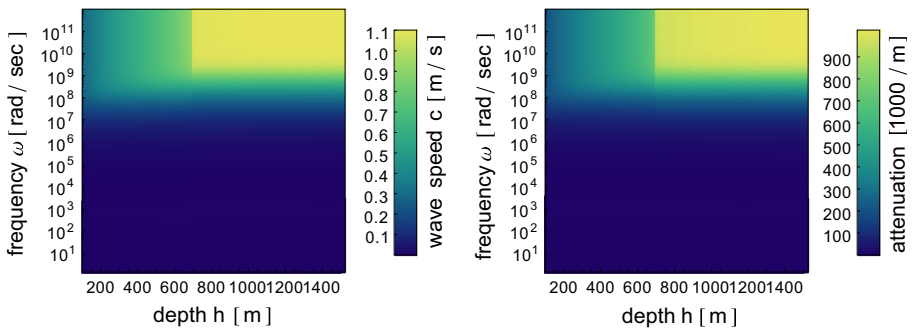

Fig. 3 First mode pressure wave speed (*left*) and corresponding attenuation (*right*) as a function of depth and frequency

affected by the content of the pores, and in both cases P_1 and S are only slightly attenuated, whereas P_2 and P_3 are highly attenuated.

For every mode, there is a 3D-plot for both wavespeed and attenuation. These plots are shown in Figs. 3 (P_1), 4 (P_2), 5 (P_3), and 6 (S). From these figures, we conclude that P_1, P_2, and S suddenly increase in speed by a few percent as soon as the CO_2 boils, which is at 695 m, whereas the attenuation behaves conversely only for P_1 and S. For P_2 the attenuation also increases as soon as the CO_2 boils. P_2 first decreases in speed as soon as the CO_2 boils and then continues to decrease in speed. The corresponding attenuation of P_3 behaves in the same way, like it is the case for P_2.

Fig. 4 Second mode pressure wave speed (*left*) and corresponding attenuation (*right*) as a function of depth and frequency

Fig. 5 Third mode pressure wave speed (*left*) and corresponding attenuation (*right*) as a function of depth and frequency
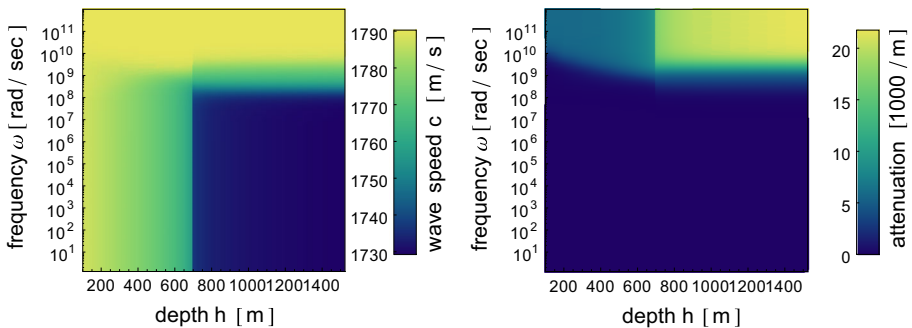
Fig. 6 Shear wave speed (*left*) and corresponding attenuation (*right*) as a function of depth and frequency

5 Discussion

We determined that the wave speed of P_1 decreases by about 15% and that of P_2 decreases by about 95% if CO_2 is present. When analyzing real data, this change in wave speed of P_1 is not necessarily related to a pore-content change, because this could also be explained, for example, by a change in the elastic moduli of the rock. The existance of a third mode could

provide evidence of an additional phase in the pores, but P_2 and P_3 are very slow and highly attenuated. This makes it difficult to detect these phases directly.

Previously, among others, Albers (2009) and Santos et al. (1990a, b) dealt with similar problems, although they used different approaches and calculated wave speeds and attenuation for different scenarios. Interestingly, Albers (2009) calculated very similar values for a sandstone filled with an air-water mixture (Albers 2009, Fig. 4) using an approach based on a macroscopic linear model, which accommodates both the Biot model and the Simple Mixture Model of Wilmanski (1998). For the Lagrangian derivation of Santos et al. (1990a), a thermodynamic approach including the principle of virtual complementary work and energy density functions was used. They computed wave speeds for oil-water mixtures in two different sandstone formations (Santos et al. 1990b). The derivation of our equations is loosely based on Coussy (2004). The advantage of our work is that we only use the balances of mass (Eq. 1) and linear momentum (Eqs. 14 and 15), as well as an equation which is based on the equations of state (Eq. 8) and Darcy's law (Eq. 17). This makes our derivation clear and simple. Nevertheless, the similarity of our numerical results with the results from Albers (2009) and Santos et al. (1990a, b) indicates that our approach is consistent with their work.

6 Conclusion

We have presented an extension of Biot's theory valid for unsaturated porous media with two different pore-space phases. We found that for each additional fluid phase there is an additional pressure wave (i.e., the number of different kinds of pressure waves is $\alpha + 1$).

We tested this extension for a representative CO_2-storage scenario to assess whether it is possible to detect leakage of a CO_2-storage site. Our results suggest that it will be difficult to detect the P_3-wave because it is very slow and highly attenuated. More promising attempts involve detection of changes in P_1 and P_2 wave speeds induced by a leak. This requires a baseline seismic survey before injection and comparison of subsequent surveys to the baseline, i.e., time-lapse seismic migration (Carcione et al. 2006). Another approach involves cross-well monitoring (Morency et al. 2011).

References

Aki, K., Richards, P.G.: Quantitative Seismology, 2nd edn. University Science Books, Sausalito (2002)

Albers, B.: Analysis of the propagation of sound waves in partially saturated soils by means of a macroscopic linear poroelastic model. Transp. Porous Media **80**(1), 173–192 (2009)

Biot, M.A.: Theory of elasticity and consolidation for a porous anisotropic solid. J. Appl. Phys. **26**(2), 182–185 (1955)

Biot, M.A.: Theory of propagation of elastic waves in a fluid-saturated porous solid. I. Low-frequency range. J. Acoust. Soc. Am. **28**(2), 168–178 (1956a)

Biot, M.A.: Theory of propagation of elastic waves in a fluid-saturated porous solid. II. Higher frequency range. J. Acoust. Soc. Am. **28**(2), 179–191 (1956b)

Brooks, R.H., Corey, A.T.: Hydraulic properties of porous media. Hydrology Papers 3, Colorado State University, Fort Collins (1964)

Carcione, J.M., Picotti, S., Gei, D., Rossi, G.: Physics and seismic modeling for monitoring CO_2 storage. Pure Appl. Geophys. **163**(1), 175–207 (2006)

Coussy, O.: Poromechanics. Wiley, Chichester (2004)

Gor, G.Y., Prévost, J.H.: Modeling CO_2-water leakage from geological storage involving phase transitions. Unpublished report, Department of Civil and Environmental Engineering, Princeton University (2014)

Jeffreys, H., Jeffreys, B.S.: Methods of Mathematical Physics, 2nd edn. Cambridge University Press, Cambridge (1950)

Kopp, A., Class, H., Helmig, R.: Investigations on CO_2 storage capacity in saline aquifers: Part 1. Dimensional analysis of flow processes and reservoir characteristics. Int. J. Greenh. Gas Control **3**(3), 263–276 (2009)

Lo, W.C., Sposito, G., Majer, E.: Wave propagation through elastic porous media containing two immiscible fluids. Water Resour. Res. **41**, W02025 (2005)

Morency, C., Luo, Y., Tromp, J.: Acoustic, elastic and poroelastic simulations of CO_2 sequestration crosswell monitoring based on spectral-element and adjoint methods. Geophys. J. Int. **185**, 955–966 (2011)

Neumann, S.P.: Theoretical Derivation of Darcy's Law. Acta Mech. **25**(3–4), 153–170 (1977)

Pini, R., Krevor, S.C.M., Benson, S.M.: Capillary pressure and heterogeneity for the CO_2/water system in sandstone rocks at reservoir conditions. Adv. Water Resour. **38**, 48–59 (2012)

Plug, W.J., Bruining, J.: Capillary pressure for the sand-CO_2-water system under various pressure conditions. Application for CO_2 sequestration. Adv. Water Resour. **30**, 2339–2353 (2007)

Prévost, J.H.: Dynaflow: A Nonlinear Transient Finite Element Analysis Program (1981). http://www.blogs.princeton.edu/prevost/dynaflow/ (last update 2012)

Santos, J.E., Corber, J., Douglas Jr, J.: Static and dynamic behavior of a porous solid saturated by a two-phase fluid. J. Acoust. Soc. Am. **87**(4), 1428–1438 (1990a)

Santos, J.E., Douglas Jr, J., Corber, J., Lovera, O.M.: A model for wave propagation in a porous medium saturated by a two-phase fluid. J. Acoust. Soc. Am. **87**(4), 1439–1448 (1990b)

Span, R., Wagner, W.: A new equation of state for carbon dioxide covering the fluid region from the triple-point temperature to 1100 K at pressures up to 800 MPa. J. Phys. Chem. Ref. Data **25**(6), 1509–1596 (1996)

van Genuchten, M.T.: A closed-form equation for predicting the hydraulic conductivity of unsaturated soils. Soil Sci. Soc. Am. J. **44**(5), 892–898 (1980)

Wilmanski, K.: Thermodynamics of Continua. Springer, Berlin (1998)